

Symmetric C–C Stretching Mode Splitting versus CH₂-Chain Conformation Order in Sodium Montmorillonite Modified by Cetyltrimethylammonium Bromide

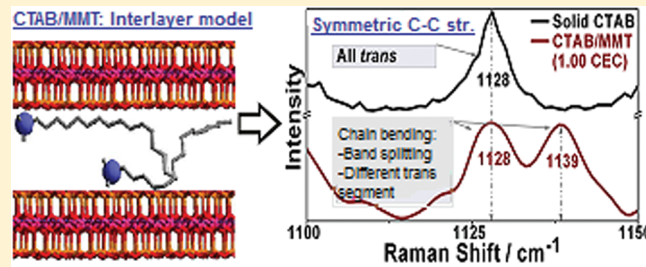
Elena A. Sagitova,^{*†,‡} Patrice Donfack,[‡] Kirill A. Prokhorov,[†] Goulnara Yu. Nikolaeva,[†] Viktor A. Gerasin,[§] Nadezhda D. Merekalova,[§] Arnulf Materny,[‡] Evgeny M. Antipov,[§] and Pavel P. Pashinin[†]

[†]A.M. Prokhorov General Physics Institute of Russian Academy of Sciences, Moscow, Russia

[‡]Physics Department, Center of Functional Materials and Nanomolecular Science, Jacobs University, Bremen, Germany

[§]A.V. Topchiev Institute of Petrochemical Synthesis of Russian Academy of Sciences, Moscow, Russia

ABSTRACT: Exploiting Raman spectroscopy and computational modeling, for the first time, we report and explain an interesting phenomenon in clay modified by cetyltrimethylammonium bromide. A splitting of the CH₂-chain's symmetric C–C stretching Raman mode found at $\sim 1128 \text{ cm}^{-1}$ in cetyltrimethylammonium bromide into two bands at 1128 and 1139 cm^{-1} in clay modified by cetyltrimethylammonium bromide is observed. We demonstrate that this splitting appears if two types of *trans*-segments with nonequivalent lengths and terminal groups coexist in the CH₂-chain of the alkylammonium ion embedded into the clay interlayer space. We report Raman experimental evidence for a CH₂-chain bending within the clay galleries, resulting in the symmetric C–C stretching band splitting, as was also suggested by computational modeling. Noteworthy, we postulate that this unique behavior based on CH₂-chain bending provides a general understanding of conformation reorganization and switching within long CH₂-chain molecules confined within modified clay interlayer galleries. For all modifier concentrations, we show that the intercalated cetyltrimethylammonium ions exist in a liquid-like state, consisting mainly of *trans* conformations ($\sim 86\%$) of two types in approximately equal proportions. Moreover, we demonstrate that the integral Raman intensity ratio $I_{1295}(\text{CH}_2)/I_{705}(\text{clay})$ provides a rapid nondestructive quantification of the relative content of alkylammonium ions in modified clays. These results demonstrate that a simple direct monitoring of specific modifier-dependent interlayer conformational states is possible, which is of great importance for a tunable fabrication of modified clays-based nanocomposites with desired properties.



1. INTRODUCTION

Clays modified by alkylammonium ions serve as easily accessible and convenient models for biomembranes.¹ In industry, they are used as fillers for polymer–clay nanocomposites^{2–5} and absorbents for the treatment of contaminated waste streams.⁶ The alkylammonium ions in the modified clay are intercalated in the spaces between silicate plates of clay crystallites (these spaces are clay interlayer galleries). During such an embodiment, CH₂-chains of the ions can undergo self-reorganization and adopt various conformations in the galleries.^{2–4,7–11} The type of the actual conformations depends on the chemical composition and content of the modifier.^{3,7–10} In return, the properties of the modified clays depend strongly on the state of the alkylammonium ions in the clay galleries.^{3,4,7} Therefore, the knowledge of CH₂-chain conformations in the modified clay is of great importance for many scientific and industrial applications.

Currently, there are still gaps in the knowledge about CH₂-chain conformations in the modified clays in many aspects. This incomplete knowledge is due to the insensitivity of traditional experimental methods, including X-ray diffraction and differential scanning calorimetry (DSC), to conformational states of the

intercalated ions. It is well-known that Raman scattering and IR absorption are widely used to probe conformations of different organic molecules. However, due to strong fluorescence from clays in the visible spectral region and their complex (overlapping bands) IR spectra, most Raman^{9,10} and IR absorption^{8,11} studies of modified clays had been long time restricted to the wavenumber region between 2750 and 3200 cm^{-1} . As we have discussed in a recent report,⁷ in this region, Raman and IR adsorption spectra provide only a qualitative characterization of the conformational order, but quantitative analysis is rather difficult due to overlapping bands.^{8–11}

Recently, we have applied Raman spectroscopy in the spectral region [600–1600 cm^{-1}] for the monitoring of the interlayer structure of sodium montmorillonite clay ($\text{Na}^+ - \text{MMT}$) modified by ditetradecyldimethylammonium bromide (DDAB, $[(\text{CH}_3(\text{CH}_2)_{13})_2\text{N}^+(\text{CH}_3)_2\text{Br}^-]$).⁷ We found that the region [600–1600 cm^{-1}] is an interesting fingerprint domain, which

Received: August 20, 2011

Revised: November 30, 2011

Published: December 02, 2011

contains many spectral features relevant for both qualitative and quantitative characterization of the conformational states of CH₂-chains in the interlayer space of the fillers. The features can be used to check results of simulating models concerning ditetradecyldimethylalkylammonium ions (DDA⁺) conformations in the clay.

Also, for Na⁺-MMT modified by DDAB, we have found an interesting and unexpected behavior of the band at about 1130 cm⁻¹, which corresponds to the symmetric C-C stretching vibrations of *trans*-segments in CH₂-chains. We have observed a unique band at 1133 cm⁻¹ in the Raman spectra of the ditetradecyldimethylalkylammonium ions (DDA⁺)/clay (DDA⁺-MMT) hybrids having the lowest alkylammonium ions content and two lines at 1124 and 1135 cm⁻¹ at the highest alkylammonium ion content, which are also present in the Raman spectrum of solid DDAB. We have explained this phenomenon by the existence and the reorganization in the clay interlayer galleries of certain types of the intercalated CH₂-chain *trans*-segments, which differ in their lengths and in their terminal groups. Especially, two critical conformations of alkylammonium ions in the DDAB-MMT composites could be recognized. One of the conformations consists of two identical -(CH₂)₁₃-CH₃ *trans*-segments with a common terminal (CH₃)₂-N- group and exists at low modifier content. The second one is the crystal-like conformation consisting of two nonequivalent *trans*-segments¹² >N-(CH₂)₁₃-CH₃ and -(CH₂)₉-CH₃, which give rise to the splitting of the 1130 cm⁻¹ band into the two lines at 1124 and 1135 cm⁻¹ at high modifier contents.⁷ Furthermore, in our previous Raman study⁷ of solid dioctadecyldimethylammonium bromide (DODAB, [(CH₃(CH₂)₁₇)₂N⁺(CH₃)₂Br⁻]), we have found that the low-intensity, broad, and asymmetric band at approximately 1130 cm⁻¹ in the Raman spectrum of solid DODAB is a superposition of two bands with wavenumbers 1127 and 1135 cm⁻¹. These two bands correspond to symmetric C-C stretching vibrations in two nonequivalent *trans*-segments¹⁴ >N-(CH₂)₁₇-CH₃ and -(CH₂)₁₃-CH₃, respectively, as was also discussed in our recent work about MMT modified by DDAB.⁷

Numerous experimental and theoretical studies about the spectral characteristics (band position and shape) of the symmetric C-C stretching Raman mode of CH₂-chains for different substances (*n*-alkanes, fatty acids, *n*-alkylamines, polyethylene, alkylammonium salts, etc.) have also been reported.^{13,15-25} Nevertheless, except our Raman study,⁷ only Kalyanasundaram and Thomas¹³ also observed two low-intensity bands at the wavenumbers 1126 and 1142 cm⁻¹ in the Raman spectrum of the micellar form of cetyltrimethylammonium bromide (CTAB, [CH₃(CH₂)₁₅N⁺(CH₃)₃Br⁻]) in contrast to a high-intensity single band at 1128 cm⁻¹, which is present in the spectrum of solid CTAB. However, there was no interpretation of this experimental observation. Thus, the behavior of the symmetric C-C stretching mode in the Raman spectra of alkylammonium-clay hybrid systems and other alkylammonium substances is of paramount interest and should be investigated and understood in more detail.

In the present work, we carry out a detailed (experimental and numerical) investigation of the symmetric C-C stretching mode in clays modified by CTAB. CTAB as opposed to DDAB has one CH₂-chain in a molecule. Comparison of Raman and numerical data for DDAB and CTAB guest molecules can provide a great understanding of the complex structure of the modified clays.

The choice of this material has been motivated by the following reasons. The structure of the clays modified by CTAB

is well studied by different experimental methods including X-ray diffraction and DSC⁴ and Raman spectroscopy¹⁰ in the region 2700–3200 cm⁻¹. Moreover, there are several conformational models²⁶ of organic layers (pseudotrilayer, lateral monolayer, paraffin-type monolayer), which CH₂-chains of CTAB ions can form in the interlayer space of the clays. According to the outcome of such modeling, the nonequivalency in lengths of *trans*-segments appears in CH₂-chains of organic pseudotrilayer as a result of some form of bending of the CH₂-chains in the CTA⁺ ions. However, there have not been any supporting experimental proofs of the existence of such computer-simulated CH₂-chain conformational states in clays modified by CTAB. As demonstrated in our previous report about DDA⁺-MMT composites,⁷ we believe that the monitoring of the symmetric C-C stretching Raman mode can allow us to probe the new structural information about CH₂-chain conformations of the clays modified by CTAB. Given the already suggested chain bending based on modeling,²⁶ we aim to show that CH₂-chain bending provides the basis for the unique band behavior of the C-C symmetric stretching mode and for a general understanding of conformation reorganization and switching within long CH₂-chain molecules confined into the interlayer galleries of modified clays.

2. MATERIALS AND METHODS

2.1. Materials Preparation. In the present work, we perform Raman measurements of sodium montmorillonite (Na⁺-MMT with 95 mg equiv/100 g of cation exchange capacity (CEC)) modified with variable mass content of CTAB (98% purification, produced by "Carl Roth, Karlsruhe, Germany"). The mass contents of cetyltrimethylammonium ions (CTA⁺) in the produced CTA⁺-MMT hybrid systems were 13% (0.50 CEC), 18% (0.75 CEC), 22% (1.00 CEC), 30% (1.50 CEC), and 37% (2.00 CEC). The numbers in brackets give the CTA⁺ contents expressed in the cation exchange capacity of the clay.

The modified clay samples were prepared through a cation-exchange reaction in hot aqueous suspensions as described in our previous reports.^{4,7} The mass content of the CTA⁺ ions in the obtained suspensions of CTA⁺-MMT was determined after 48 h following the preparation of the suspensions using an original method described in detail earlier.⁴ To produce the CTA⁺-MMT samples, we used a hot aqueous solution (70–80 °C) with a CTAB concentration of 2.5 × 10⁻³ mol/L.

For X-ray diffraction and DSC measurements, CTA⁺-MMT sample aliquots taken from the obtained suspensions were deposited on glass plates and dried in an evacuated oven. As far as probes for Raman measurements were concerned, the CTA⁺-MMT suspensions were simply dried, and the obtained powder was pressed into small tablets for 5 min under a pressure of 3 MPa.

2.2. X-ray Diffraction and DSC Characterization. All CTA⁺-MMT samples used for the present study were initially characterized by X-ray diffraction and DSC. These X-ray diffraction and DSC measurements were described in detail earlier.⁴ In brief, X-ray spectra of the CTA⁺-MMT samples were taken with a DRON-3 spectrometer (DRON-3, Bourevestnik Inc., St. Petersburg, Russia) with a Cu K α excitation at 0.154 nm, monochromated by a graphite monocrystal. Thermograms of the CTA⁺-MMT samples were measured using a DTAS-1300 differential scanning microcalorimeter (DTAS-1300, Samara, Russia) in the temperature range from 10 to 180 °C, with a heating rate of 8 °C/min and about 20 mg of weighted samples.

2.3. Numerical Simulation Modeling. For the CTA⁺–MMT sample with CTA⁺ ions content of 0.75 CEC, we have carried out computer-simulation modeling. The procedure of the computer-simulation modeling was described in detail in a previous study on DDA⁺–MMT hybrids.⁷ In particular, the description of the potential energy of CTA⁺–MMT hybrid system, the parameters of the force field, and the methods for the construction of the MMT-surface and modifier, which we used in this study, were identical to what we used for computer-simulation modeling of the DDA⁺–MMT hybrids.⁷ In brief, the computer-simulation modeling of CTA⁺ ion conformations in modified clay tactoids was carried out by molecular dynamics (MD) methods based on the minimization of the potential energy. The potential energy of modified clay was described as follows:

$$E_{\text{CTA}^+-\text{MMT}} = E_{\text{MMT}} + E_{\text{CTA}^+} + E_{\text{MMT,CTA}^+} \quad (1)$$

where $E_{\text{CTA}^+-\text{MMT}}$, E_{MMT} , and E_{CTA^+} are the potential energies of CTA⁺–MMT, MMT tactoids, and CTA⁺, respectively. The $E_{\text{MMT,CTA}^+}$ is the energy of interaction between MMT and CTA⁺.

For the construction of the MMT-surface, we have used a 3D periodical crystal structure with the surface sizes 3.10 nm × 1.64 nm. The initial distance between two neighboring parallel silicate plates was variable, depending on the initial input conditions (e.g., tilt angle of the embedded CTA⁺ ions with respect to a given silicate plate, their initial localization in the plane of the plate, etc.). To obtain equilibrium CTA⁺–MMT systems, we first performed 100–300 ps NVT (constant temperature and constant volume) MD simulations at 375 K with time steps of 0.001 ps.

At the next step of our simulations, we carried out NPT (isobaric–isothermal ensemble) MD calculations with duration of 100–300 ps, at atmospheric pressure, and at $T = 350$ K.

2.4. Raman Experiments. To record Raman spectra of modified clays (CTA⁺–MMT), we used the 488.0 nm line of an Ar⁺ laser source (Innova 308 series, Coherent, U.S.) for excitation. The scattered light was analyzed in a Triax monochromator (TRIAx 550, Jobin Yvon, France) using a 1200 grooves per mm diffraction grating and a slit width of 100 μm . A liquid N₂ cooled CCD detector (CCD 3500, Jobin Yvon, France) was used for signal detection. The laser power at the sample did not exceed 4 mW. The scattered light was collected in the backscattering geometry using a 100× (N.A. 0.95) and a 40× (N.A. 0.65) lens for nonpolarized and polarized Raman spectra, respectively. Spectra were recorded with exposure times from 20 to 120 s and accumulated over 2–10 times depending on the sample. Rayleigh scattering rejection was achieved by mounting a holographic Notch filter in front of the spectrometer before focusing the Raman signal onto the spectrometer slit using a bi-convex lens with 10 cm focal length. Signal polarization components were selected by a filter placed in the scattered light beam.

The scattering geometry for polarization-dependent measurements corresponds to the laboratory coordinates system, where the Z-axis is parallel to the wave vectors of the exciting and scattered radiations. The electric field vectors of the exciting and collected scattered radiations were polarized along the X-axis. The locations of the focus of the laser beam were different for nonpolarized and polarized measurements, because these measurements were carried out independently, but spectra were recorded from many sampling points (~ 5) on each sample (to ensure that point to point variation was negligible) and averaged. Note that our TRIAX 550 Raman setup (described above) used

for recording both polarized and nonpolarized spectra of CTA⁺–MMT shows little dependence on the polarization of the scattered light. For nonpolarized spectra, the relative contribution of the $Z(X,X)Z$ -scattering with respect to $Z(X,Y)Z$ -scattering was equal to 1.28.

For the interpretation of the Raman spectra of the modified clays, we also recorded reference Raman spectra of polyethylene (PE), *n*-alkanes [C_nH_{2n+2} , $n = 5–17$], primary *n*-alkylamines [$C_nH_{2n+1}N^+H_3Cl^-$, $n = 6, 8, 12$], and quaternary alkylammonium salts (CTAB (the modifier), DODAB, DDAB). To record reference Raman spectra, we used the 488.0 nm excitation line of an Ar⁺–Kr⁺ laser (Stabilite 2018, Spectra-Physics, U.S.) and a double monochromator (U1000, Jobin Yvon, France) equipped with two plane holographic diffraction gratings with 1800 grooves per mm, four slits with the width set to 300 μm , and a photomultiplier detector cooled by water, all assembled to achieve a 90° scattering geometry. Note that the spectral resolution was estimated to be ~ 2 cm^{-1} for Raman spectra of the modified clays (on the TRIAX 550 Raman setup) and 3 cm^{-1} for the aforementioned reference Raman spectra measured on a different Raman system (the U1000 Raman setup). The aromatic breathing mode of toluene at 1003.7 cm^{-1} was used for wave-number calibration of the different Raman spectrometers.

Spectral analysis was performed using two curve-fitting routines as described in detail in a previous work.⁷ These two routines made use of the NGLabSpec software package for automatic spectra acquisition and analysis and of a homemade program based on a nonlinear least-squares fitting and the Levenberg–Marquardt algorithm. Both routines provided spectra deconvolution via a weighted sum of Gaussian and Lorentzian functions. Before fitting, a fourth-order polynomial background fit was first subtracted from the experimental spectra. The results of the two ways of spectra deconvolution have coincided within the accuracy of the Raman measurements.

2.5. Fitting of the Experimental Data by an Irrational Function (a Function Involving an Irrational Number). We have applied a mathematical treatment (least-squares regression with previous linearization of the regression function) to analytically describe, by a function involving an irrational number (see eq 2), the experimental dependence $\{Y_i(X_i)\}$ of the wave-number of the symmetric C–C stretching mode on the *trans*-segment length as follows:

$$y(x) = \sqrt{P_1^2 + P_2^2 \sin^2 \frac{\pi}{x}} \quad (2)$$

Here, the set $\{Y_i(X_i)\}$ represents the experimental data consisting of k data pairs (x_i, y_i) , $i = 1, 2, \dots, k - 1, k$. The x_i or x are independent variables, and the y_i or y depend on x_i or x , respectively. The values y_i are determined by experimental observations. P_1^2 and P_2^2 are the fitting constants. The fitting procedure includes three steps. First, the linearization of eq 2 was made. A data set $\{Y_i^*(X_i)\}$ is created, which consists of n data pairs (x_i, y_i^*) , where $y_i^* = y_i^2$. Expression 2 then is rewritten in the following equivalent form:

$$y^*(x) = \theta_1 + \theta_2 \sin^2 \frac{\pi}{x} \quad (3)$$

where $\theta_1 = P_1^2$ and $\theta_2 = P_2^2$.

Finally, we use the least-squares regression method to find the coefficients θ_1 and θ_2 , and then to explicitly express the data

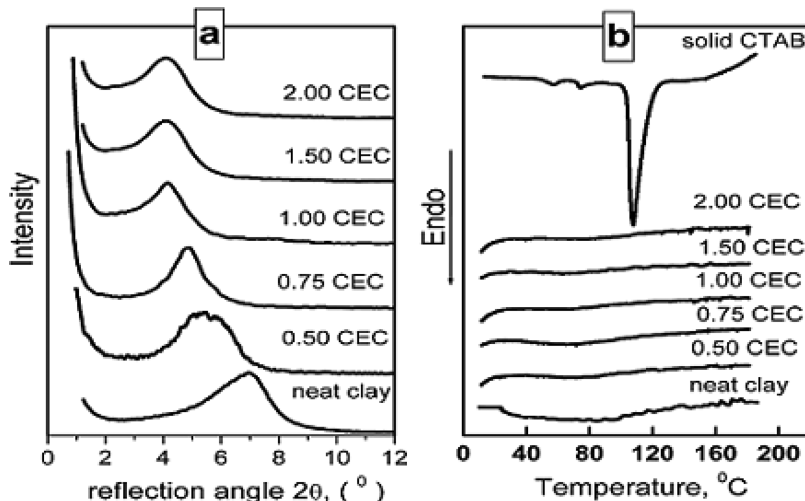


Figure 1. X-ray spectra (a) and DSC thermograms (b) of MMT clay modified by CTAB.

fitting expression 2 from expression 3 with the obtained coefficients θ_1 and θ_2 .

3. RESULTS AND DISCUSSION

3.1. Interlayer Structure Computational Models of CTA⁺-MMT Hybrids Consistent with X-ray Diffraction and DSC Characterization. Figure 1 shows X-ray spectra (a) and DSC thermograms (b) of MMT clay modified by CTAB. In agreement with our previous DSC studies,⁴ no trace of CTA⁺ melting could be detected for any CTA⁺ content in the thermograms of CTA⁺-MMT hybrids. Therefore, the state of CTA⁺ ions in these hybrids is liquid-like. Table 1 summarizes the heights of the clay interlayer space “ d_{001} ” revealed by X-ray diffraction, and the types of CTA⁺ layers in the CTA⁺-MMT composites. The types of CTA⁺ layers in the CTA⁺-MMT were determined by the comparison of the d_{001} heights with the geometric sizes of CTA⁺ molecular conformation, in which the segment $-\text{N}-\text{C}_{16}\text{H}_{33}$ is assumed to adopt the “all-trans” conformation.

The d_{001} heights at CTA⁺ ion contents of 0.75 CEC and below correspond to twice the cross size of the CTA⁺ ion if its CH₂-chain is parallel to a silicate plate. Therefore, according to X-ray diffraction data and assuming an all-trans conformation of the intercalated CH₂-chains, the CTA⁺ ions embedded in the clay interlayer spaces form bilayers at CTA⁺ ion contents equal to or below 0.75 CEC. In these bilayers, the all-trans CTA⁺ chains are parallel to each other. Figure 2a shows the model of bilayer packing of CTA⁺ ions in the clay interlayer spaces, in the case where the CH₂-chains in the CTA⁺ ions have all-trans conformation. In addition, Figure 2b shows the alternative model of CH₂-chain conformations for bilayer packing, in which two types of trans-segments appear as the result of the bending of the chain of CTA⁺. trans-Segments of the first type consist of a segment of “ k ” CH₂-groups [(-CH₂) _{k}] together with a terminal (CH₃)₃-N– unit. The trans-segments of the second type contain only CH₂-groups without the terminal (CH₃)₃-N– unit. Both packing models arise from computer simulations and are discussed in the next section.

The CTA⁺ ion pseudotrilayers are formed between silicate clay plates, when the CTA⁺ ion contents are equal to or greater than 1.00 CEC, because in this case, the d_{001} heights correspond

Table 1. X-ray Diffraction Data for the Modified Clays CTA⁺-MMT

CTA ⁺ ion content			
cation exchange capacity of modified clay (CEC)	relative mass ratio CTA ⁺ /MMT	height of the clay interlayer space d_{001} (nm)	type of structure of the clay interlayer space
0 (neat clay)	0	1.25	empty layers
0.50	0.15	1.7	bilayers
0.75	0.22	1.8	bilayers
1.00	0.29	2.1	pseudotrilayers
1.50	0.44	2.1	pseudotrilayers
2.00	0.58	2.1	pseudotrilayers

to more than twice the cross size of the CTA⁺ ion when its CH₂-chain is parallel to a silicate plate.

X-ray diffraction data allow reducing the number of simulated optimum configurations of the packing of CTA⁺ ions by applying the appropriate limiting condition. An important boundary condition is that the computer-simulated d_{001} heights must coincide with the experimentally measured values of d_{001} heights provided by X-ray diffraction. However, within these limits, there are still several models of CTA⁺ ion bilayer packing applicable. These models differ in the various conformations of embedded CH₂-chains, but possess the same d_{001} height and the same total potential energy of CTA⁺-MMT. In particular, the two bilayer packing models briefly mentioned above and displayed in Figure 2 demonstrate such degenerate models, which were simulated with different initial localizations of the embedded CTA⁺ ions relative to the plane of a silicate plate. Other initial conditions, including the tilt angle to the silicate plate and the conformation (all-trans) of CH₂-chains in CTA⁺ ions, were the same for both models. Trying 10 different initial localizations of the CTA⁺ ions relative to the silicate plate, we have found that the expectancy values of the models described by Figure 2a and b are 20% and 80%, respectively. However, this result does not allow one to prefer one model to the other, because the predicted expectancy strongly depends on initial conditions for the computational modeling. Noteworthy, we show that the monitoring

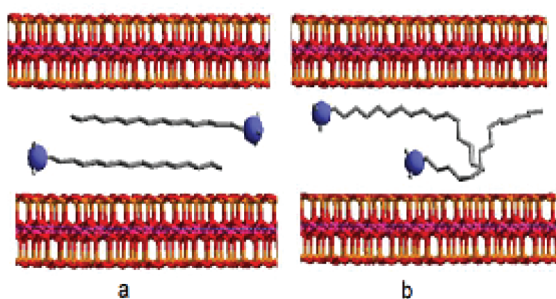


Figure 2. Computer-simulated models of alkyl chain conformations for CTA^+ -MMT with 0.75 CEC of CTA^+ corresponding to the same height of the interlayer space. Model (a) is confirmed by X-ray diffraction, while model (b) is confirmed by both X-ray diffraction and Raman spectroscopy, and, in both models, the sheets, filled balls, and zigzag lines represent the silicate plates, $-\text{CH}_2-\text{N}-\text{(CH}_3)_3$ groups, and alkyl chains of CTA^+ ions, respectively.

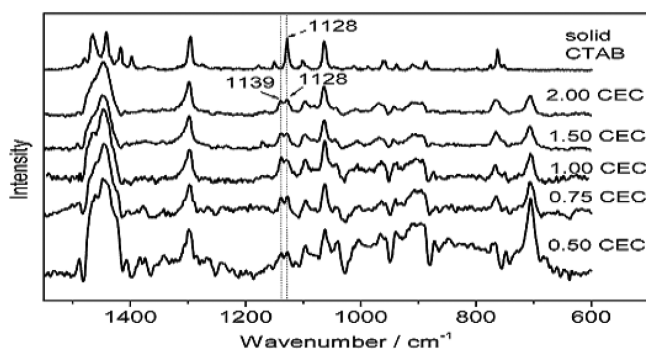


Figure 3. Nonpolarized Raman spectra of the modified clay CTA^+ -MMT with CTA^+ ion content from 0.50 to 2.00 CEC and of solid CTAB (topmost) in the region $600-1550 \text{ cm}^{-1}$.

of the symmetric C-C stretching band in the Raman spectra allows for the selection of the most realistic models of CTA^+ ion conformations and finally the determination of the correct models for intercalated CTA^+ ion packing within clay interlayer galleries.

3.2. Raman Characterization of the Conformational Order.

Figure 3 shows nonpolarized Raman spectra of CTA^+ -MMT with different mass contents of CTA^+ ions and of solid CTAB in the region [$600-1550 \text{ cm}^{-1}$]. All spectra are normalized to the peak intensity of the CH_2 -twisting Raman band at 1295 cm^{-1} . This band in the Raman spectra of molecular systems containing CH_2 -chains is a superposition of twisting vibrations of CH_2 groups both in *trans*- (with the wavenumber 1295 cm^{-1}) and in *gauche*- (with the wavenumber 1305 cm^{-1}) conformers. As a matter of fact, the integral intensity of the CH_2 twisting band is proportional to the total content of CH_2 groups in CH_2 -chains¹⁵ and provides a straightforward quantification of the modifier content. The isolated band at 705 cm^{-1} in the Raman spectra of CTA^+ -MMT is exclusively due to clay and is assigned to the $\nu_1(\text{A}_1)$ vibrational mode of SiO_4 -tetrahedrons in clay silicate plates.²⁷ Other Raman bands in the region [$600-1550 \text{ cm}^{-1}$] are attributed to vibrations of various structural units in CTA^+ ions.^{7,13,16-23} Both the CH_2 -twisting (mentioned above) and the C-C stretching vibrations of CH_2 -chains are expected in the spectral region [$1000-1350 \text{ cm}^{-1}$].^{7,13,16-23} The spectral region below 1000 cm^{-1} belongs to the vibrational fingerprint region of the hydrocarbon

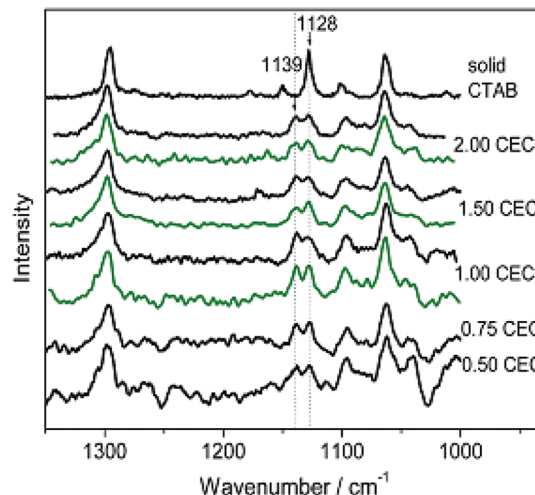


Figure 4. Nonpolarized (black) and polarized (green) Raman spectra of the modified clay CTA^+ -MMT with CTA^+ ion content from 0.50 to 2.00 CEC and the nonpolarized Raman spectrum of solid CTAB (topmost) in the region $1000-1350 \text{ cm}^{-1}$.

“tails” $-\text{CH}_2-\text{CH}_3$ and “heads” $-\text{CH}_2-\text{N}-\text{(CH}_3)_3$.^{13,17-19} The bands within about $1400-1470 \text{ cm}^{-1}$ are assigned to different bending vibrations of $-\text{CH}_2$ and $-\text{CH}_3$ groups.^{13,16}

Figure 4 depicts nonpolarized and polarized Raman spectra of CTA^+ -MMT under study and solid CTAB in the region [$1000-1350 \text{ cm}^{-1}$]. The nonpolarized spectra in Figure 4 have been extracted from Figure 3. For polarization-dependent Raman investigations, the Raman spectra of the CTA^+ -MMT samples corresponding to CTA^+ mass content from 1.00 to 2.00 CEC are discussed. The polarized Raman spectra of other CTA^+ -MMT samples (mass content below 1.00 CEC) showed a low signal-to-noise ratio. The reason for this is that the inelastically scattered signal from CTA^+ -MMT is rather weak. In addition, the signal, which becomes even weaker as a result of reduced mass content of CTA^+ ions and the underlying strong clay fluorescence, is further reduced by the polarizer film placed in the signal beam.

The sharp and highly intense band at 1128 cm^{-1} in the Raman spectrum of solid CTAB corresponds to the symmetric C-C stretching Raman mode in *trans*-segments of CH_2 -chains in CTAB. As in our previous Raman study on Na^+ -MMT modified by DDAB,⁷ briefly mentioned in the introduction, we have also found a very interesting and unexpected behavior of the band at about 1128 cm^{-1} in the Raman spectra of CTA^+ -MMT. It is worth mentioning that solid CTAB is structurally quite different from solid DDAB, and such a difference is also reflected in their Raman signatures around the symmetric C-C stretching mode in *trans*-segments. Yet surprisingly, the 1128 cm^{-1} band behaves similarly. In both nonpolarized and polarized Raman spectra of CTA^+ -MMT, instead of a single high-intensity Raman band at 1128 cm^{-1} , we have observed a doublet of two relatively weak bands with peak wavenumbers at 1128 and 1139 cm^{-1} (Figure 4).

Unlike the difference in the crystal structure between CTAB and DDAB, the appearance of this doublet in CTA^+ -MMT as well is a rather interesting phenomenon, suggesting a unique nature of the behavior of *trans*-segments in CH_2 -chains of clay/alkylammonium hybrids, as we will demonstrate later.

3.3. Origin of the 1128/1139 Doublet and the Associated Conformational Order in Clays Modified by CTAB.

The peak

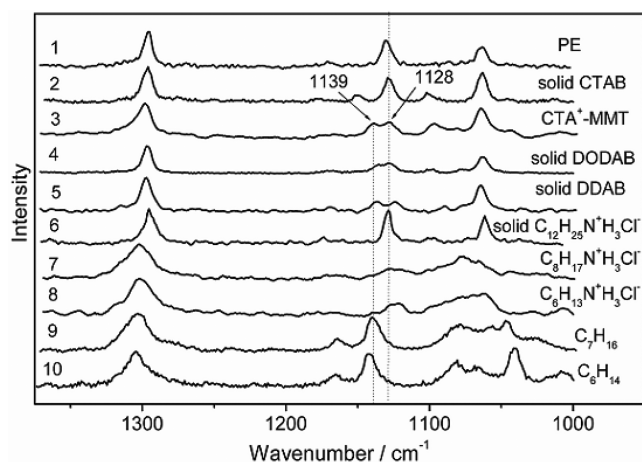


Figure 5. Raman spectra of substances containing alkyl chains, including PE (1), CTAB (2), CTA⁺-MMT (3) with CTA⁺ content of 2.00 CEC, DODAB (4), DDAB (5), primary *n*-alkylamines (6–8), and *n*-alkanes (9,10).

positions 1128 and 1139 cm⁻¹, determined directly from the experimental spectra (without any spectra deconvolution), are marked in the nonpolarized Raman spectra of solid CTAB and CTA⁺-MMT with 2.00 CEC of CTA⁺ ion mass content in Figure 3 (the two upper traces) as well as in other figures showing Raman spectra of the different substances under study. Using spectral deconvolution, the peak positions of these bands have been found to be equal to 1128.0 ± 0.5 and 1138.7 ± 0.5 cm⁻¹, respectively, in the Raman spectra of all samples of CTA⁺-MMT (i.e., at all CTA⁺ ion content). Given the fact that the spectral resolution was as good as 2 cm⁻¹, we have retained 1128 and 1139 cm⁻¹ as reliable wavenumber values of these Raman bands.

To reveal the nature of the aforementioned phenomenon associated with the 1128 cm⁻¹ band splitting, we have analyzed the behavior of the symmetric C-C stretching Raman mode in a series of substances, whose molecules contain CH₂-chains. These substances include PE, *n*-alkanes with *n* = 5–17, primary *n*-alkylamines with *n* = 6, 8, 12, and quaternary alkylammonium salts (CTAB, DODAB, DDAB). We consider PE as a model of *n*-alkane with infinite length, that is, *n* ≈ ∞.

Figure 5 compares Raman spectra of solid CTAB and CTA⁺-MMT with CTA⁺ ion content of 2.00 CEC with the spectra of PE, *n*-alkanes [C_{*n*}H_{2*n*+2}; with *n* = 6, 7], primary *n*-alkylamines [C_{*n*}H_{2*n*+1}N⁺H₃Cl⁻, *n* = 6, 8, 12], DODAB, and DDAB. We have found that the Raman shift at 1128 cm⁻¹ in the spectra of CTA⁺-MMT coincides with the wavenumber of the symmetric C-C stretching vibration in *trans*-segments of solid CTAB. At the same time, the Raman shift at 1139 cm⁻¹ in the spectra of CTA⁺-MMT coincides with the observed peak position of the same mode (symmetric C-C stretching vibration in *trans*-segments of CH₂-chains) in the Raman spectra of the *n*-alkanes C₆H₁₄ and C₇H₁₆ (compare spectrum 3 with spectra 9 and 10 in Figure 5).

As a matter of fact, on the basis of the above experimental observations, we attribute both Raman bands at 1128 and 1139 cm⁻¹ in the spectra of CTA⁺-MMT to the symmetric C-C stretching Raman mode in *trans*-segments of CTA⁺ within the modified clay. Consequently, in the Raman spectra of CTA⁺-MMT, the symmetric C-C stretching Raman mode splits into two bands

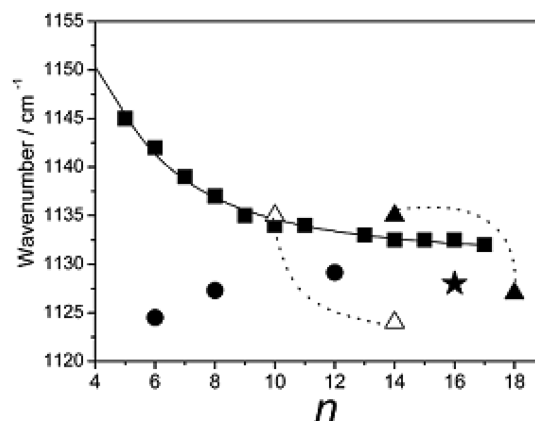


Figure 6. The Raman shifts of the symmetric C-C stretching mode versus the amount of C atoms in alkyl *trans*-segments for various substances, including *n*-alkanes (■) and the single-chain primary *n*-alkylamines (●), the single-chain CTAB (★), the double-chain DDAB (△), and the double-chain DODAB (▲). The solid line is the theoretical wavenumber law for *n*-alkanes (see text: eq 4).

forming the doublet mentioned in the previous section. To bring further evidence to this assignment and to reveal the unique structural information associated with the 1128/1139 doublet in the Raman spectra of CTA⁺-MMT, we have performed additional theoretical and experimental investigations as demonstrated in the following. According to experimental Raman studies of solid and liquid *n*-alkanes, the wavenumber of the symmetric C-C stretching mode in *trans*-segments depends on their length.^{7,19,22}

Figure 6 shows the observed peak position of the symmetric C-C stretching mode in *trans*-segments versus the number of C atoms for the different substances. Experimental data for CH₂-chain substances are shown by “■” for liquid *n*-alkanes, “●” symbols for primary *n*-alkylamines, and an “★” for CTAB. Experimental data for the solid double chain quaternary alkylammonium salts (DDAB and DODAB) are represented by “△” and “▲”, respectively. In this case, dotted lines drawn through triangle symbols indicate data attributed to one of the DDAB or DODAB molecules, each of which consists of two *trans*-chains with nonequivalent lengths (different number of C atoms). The symmetric C-C stretching mode of these double chain molecules is split into two bands in their Raman spectra (see Figure 5; traces 5 and 4). The solid line in Figure 6 represents the theoretical dependence of the symmetric C-C stretching mode wavenumber on the chain length for liquid *n*-alkanes, which we discuss below. For liquid (at normal conditions) *n*-alkanes with *n* = 5–17, we have modeled the experimental dependence of the peak position of the symmetric C-C stretching mode on the *trans*-segment length by the law expressed in eq 1 and rewritten here for convenience:

$$\nu_n = \sqrt{\nu_\infty^2 + \beta^2 \sin^2 \frac{\pi}{x}} \quad (4)$$

This wavenumber law was first suggested by Gorelik and co-workers,^{22,28} who treated the dynamics of the *quasi* one-dimensional monatomic chain with additional bonds. In eq 4, the different variables and constants involved are defined as follows: *n* is the number of C atoms in a *trans*-chain CH₃-(CH₂)_{*n*-2}-CH₃.

The ν_n and ν_∞ (expressed in cm^{-1}) are the wavenumbers of the symmetric C–C stretching mode for a finite *trans*-chain and a hypothetical infinite *trans*-chain, respectively. The *trans*-chain length L is defined by $L \approx a \cdot n/2$, where $a = 2.58 \text{ \AA}$ is the distance between two adjacent C atoms, which are localized along a straight line parallel to the axis of the *trans*-chain of *n*-alkanes. $\beta = s/a \cdot \pi \cdot c$ depends on the material, where s is the velocity of a light wave through the *trans*-chain and c is the velocity of light in a vacuum.

Using least-squares regression as described in detail earlier in section 2.5, we have calculated the values of ν_∞ and β . The obtained values are $\nu_\infty = 1130.5 \pm 0.2 \text{ cm}^{-1}$ and $\beta = 313 \pm 3 \text{ cm}^{-1}$. The calculated value $\nu_\infty = 1130.5 \pm 0.2 \text{ cm}^{-1}$ is in excellent agreement with the observed value of 1130 cm^{-1} for the wavenumber of the symmetric C–C stretching vibration of *trans*-segments in polyethylene, which can be considered to be a model substance containing infinitely long *trans*-chains. To check the calculated value $\beta = 313 \pm 3 \text{ cm}^{-1}$, we have used expression 4, substituting the coefficients $\nu_\infty = 1130.5 \text{ cm}^{-1}$ and $\beta = 313 \text{ cm}^{-1}$, to calculate the value of ν_4 (i.e., value ν_n with $n = 4$). The obtained value is $\nu_4 = 1150 \text{ cm}^{-1}$, and it is in agreement with the experimental (1150 cm^{-1}) and theoretical (1148 cm^{-1} , obtained from the valence force field computational calculations) values of the wavenumber of the symmetric C–C stretching mode in *trans*-segments of *n*-butane (C_4H_{10}) reported by Kint et al.²⁴ and Snyder.²⁵ However, we have noticed that the wavenumber law expressed in eq 4 does not straightforwardly describe the change in the wavenumber of the symmetric C–C stretching mode in the Raman spectra of primary *n*-alkylamines. First, contrary to *n*-alkanes, the observed wavenumber of the symmetric C–C stretching Raman mode in the spectra of primary *n*-alkylamines increases with the increase in the length of the *trans*-segments of the CH_2 -chain (see Figures 5 and 6). Second, we have observed that the peak positions of the symmetric C–C stretching Raman mode for primary *n*-alkylamines and *n*-alkanes are very different between molecules having the same number of C atoms. This is particularly evident when the corresponding molecules consist of short CH_2 -chains. Especially, the observed wavenumber of the symmetric C–C stretching Raman mode for the primary *n*-alkylamine with $n = 6$ ($\text{C}_6\text{H}_{13}\text{N}^+\text{H}_3\text{Cl}^-$) shifts toward the blue spectral region by approximately 17 cm^{-1} relative to that of *n*-hexane (*n*-alkane with $n = 6$, C_6H_{14}) (see Figures 5 and 6). Observations similar to those made for *n*-alkanes concerning the Raman shifts of the symmetric C–C stretching mode were reported for trimethylalkylammonium bromides by Kalyanasundaram et al.¹³ Kalyanasundaram and co-workers observed that the symmetric C–C stretching Raman band in solid CTAB appeared down-shifted by approximately 4 cm^{-1} (toward red) with respect to the position of this Raman band in solid decyltrimethylammonium bromide (DeTAB: $\text{CH}_3(\text{CH}_2)_9\text{N}^+(\text{CH}_3)_3\text{Br}^-$), whose molecule contains a shorter alkyl *trans*-chain. This result was expected because the observation is in a good agreement with the dependence of the peak position of the symmetric C–C stretching band on the CH_2 -chain length. However, in comparison to *n*-alkanes having the same length of *trans* CH_2 -chains, Kalyanasundaram et al.¹³ observed that the symmetric C–C stretching Raman band in the spectra of these trimethylalkylammonium bromides exhibited a blue wavenumber shift. The observed blue shifts were equal to 11 cm^{-1} for DeTAB with respect to *n*-decane ($\text{C}_{10}\text{H}_{22}$) and 7 cm^{-1} for CTAB with respect to *n*-hexadecane ($\text{C}_{16}\text{H}_{34}$).

We can explain the discrepancy in the behavior of the symmetric C–C stretching Raman mode in the spectra of the primary *n*-alkylamines and trimethylalkylammonium bromides in comparison to that for *n*-alkanes by the influence of a heavy terminal group ($-\text{N}^+\text{H}_3$ in primary *n*-alkylamines or $-\text{N}^+(\text{CH}_3)_3$ in trimethylalkylammonium bromides) on the collective stretching motion of the CH_2 -chain. In fact, it is well-known from Rayleigh theorem²⁹ that the wavenumber of the collective motion in a linear arrangement of masses decreases if one of the vibrational masses is replaced by a heavier mass. We have observed the most apparent situation of such wave number downshift for the primary *n*-alkylamine with $n = 6$ ($\text{C}_6\text{H}_{13}\text{N}^+\text{H}_3\text{Cl}^-$) in comparison with *n*-heptane (C_7H_{16}) (Figures 5 and 6). However, this shift in wavenumber due to heavier terminal groups is decreased if the length of *trans* CH_2 -chains increases (Figure 6). Therefore, we can postulate that, as the length of alkyl *trans*-chain increases, the influence due to the presence of a heavy terminal group on the wavenumber of the symmetric C–C stretching Raman mode in the alkyl *trans*-chains becomes negligible. This statement perfectly describes the experimental observations for substances containing CH_2 -chains with dissimilar terminal groups as depicted in Figure 6. The good confirmation of this statement lies in the fact that the splitting of the symmetric C–C stretching Raman mode nearly disappears for solid DODAB having longer *trans*-chains in comparison with solid DDAB having shorter *trans*-chains (Figures 5 and 6). Actually, as was already mentioned in the Introduction, molecules in the monocrystals of DDAB and DODAB have similar conformations, which contain two nonequivalent *trans*-segments $-(\text{CH}_2)_k-\text{CH}_3$ with terminal group $(\text{CH}_3)_2-\text{N}^+$ and $-(\text{CH}_2)_m-\text{CH}_3$ without the group $(\text{CH}_3)_2-\text{N}^+$ (where $k = 13$ and $m = 9$ for DDAB, and $k = 17$ and $m = 13$ for DODAB).^{12,14} We have found that the observed value of the splitting of the symmetric C–C stretching Raman mode is greater for solid DDAB (11 cm^{-1}) than for solid DODAB (8 cm^{-1}), whose molecule contains the longer *trans*-chains. In fact, both DDAB and DODAB are only different in the length of their double CH_2 -chains. In addition, as the chain length increases, the wavenumber of the symmetric C–C stretching Raman mode of the *trans*-segment with the heavy terminal group increases (i.e., it recovers because the influence of the heavy terminal group becomes smaller for longer chain), while the wavenumber of the other *trans*-segment without the heavy terminal group normally decreases (as discussed above and also depicted in Figure 6), resulting in the reduced splitting for DODAB as compared to DDAB.

Because of the aforementioned statements and evidence, we are now able to draw consistent conclusions about the behavior of the C–C stretching mode splitting in the spectra of CTA^+-MMT composites. Comparing the peak positions of the symmetric C–C stretching Raman mode for CTA^+-MMT , *n*-alkanes, and CTAB, we conclude the following: For the doublet observed in the Raman spectra of CTA^+-MMT , the higher-wavenumber peak at 1139 cm^{-1} is attributed to the symmetric C–C stretching vibration in *trans*-segments $-(\text{CH}_2)_k-$ with $k = 6-8$, while the lower-wavenumber peak at 1128 cm^{-1} is attributed to the symmetric C–C stretching vibration in *trans*-segments $-(\text{CH}_2)_k-\text{N}^+(\text{CH}_3)_3$ with $k = 12-15$, containing the heavy terminal group $\text{N}^+(\text{CH}_3)_3$. As a matter of fact, in the interlayer space of MMT, we have found short *trans*-segments $-(\text{CH}_2)_k-$, which consist of $6-8$ C atoms and do not contain (or equivalently, do not feel the influence of) the terminal group $\text{N}^+(\text{CH}_3)_3$.

However, unlike DDAB and DODAB, which already contain double CH_2 -chains and exhibit the symmetric C–C stretching band splitting in the solid state, the molecule of solid CTAB contains only a single *trans* CH_2 -chain with the terminal group $-\text{N}^+-(\text{CH}_3)_3$. Moreover, the splitting of the symmetric C–C stretching Raman mode is absent in the Raman spectra of solid CTAB. Taking into account both arguments, we conclude that the splitting of the symmetric C–C stretching Raman mode for the CTA^+-MMT systems is only possible due to the bending of the CTA^+ chain in the interlayer space of the MMT, providing the first Raman experimental evidence of this behavior for CTA^+ ions embedded within clay galleries, as was also predicted via computational modeling. As the result of such a bending, two *trans*-segments with nonequivalency in length and in the terminal groups are formed in the intercalated CH_2 -chains. Note that a similar conformation (two nonequivalent *trans*-segments in length and in their terminal groups) of the CH_2 -chain in CTA^+ ion was found by IR study³⁰ of cadmium thiophosphate modified by CTAB.

3.4. CH_2 -Chain Conformation Provided by the Raman Evidence of the 1128/1139 Doublet. The above-made conclusion regarding the CTA^+ chain conformation associated with the 1128/1139 doublet is in a good agreement with our results obtained from X-ray diffraction studies for the CTA^+-MMT with CTA^+ ion content greater than 1.00 CEC. This also correlates very well with the model of pseudotrilayers packing of organic chains in the interlayer space of clay.²⁶ However, regarding bilayer packing models suggested by our computational modeling for CTA^+ ion content less or equal to 0.75 CEC and displayed in Figure 2, we would like to point out again that the result of the mathematical modeling does not straightforwardly allow one to prefer one model to the other. Nevertheless, it provides some good hints (e.g., a much higher probability for the model in Figure 2b as opposed to Figure 2a: 80% vs 20%, respectively). Interestingly, a model of bilayers packing for CTA^+-MMT with low CTA^+ contents (0.75 CEC and below), in which CTA^+ chains embedded into clay interlayer space have all-*trans* conformation (Figure 2a), contradicts the observed splitting of the symmetric C–C stretching Raman-active mode (which occurs at all modifier content)! As a matter of fact, in view of our Raman data, we consider more likely the model in which intercalated chains of CTA^+ ions bend, resulting in molecular conformations with nonequal length and chemical composition of the *trans*-segments (a situation that also agrees with the higher probability for the computer-simulated packing model shown by Figure 2b). The conformations of CTA^+ chains in the model depicted by Figure 2b contain *trans*-segments of the type $(\text{CH}_3)_3\text{N}^-(\text{CH}_2)_k-$ ($k = 12-15$; with the heavy terminal group $(\text{CH}_3)_3\text{N}^-$) and of another type without the heavy terminal group, including either a $-(\text{CH}_2)_6-$ *trans*-segment in the interior or a $-(\text{CH}_2)_5-\text{CH}_3$ *trans*-segment at the end of the CH_2 -chain.

As far as polarized Raman spectra are concerned, we have in addition found that the splitting of the symmetric C–C stretching Raman-active mode is more in the polarized $Z(X,X)Z$ spectra of CTA^+-MMT in comparison with the nonpolarized spectra (Figure 4). This can be attributed to the polarization dependence of the Raman scattering for modes of different symmetry. Our TRIAX S50 Raman setup has approximately equal sensitivity for all light polarizations. In the nonpolarized spectra of CTA^+-MMT , the contributions of parallel and crossed polarization signals are comparable, while in the polarized spectra only the parallel component was detected.

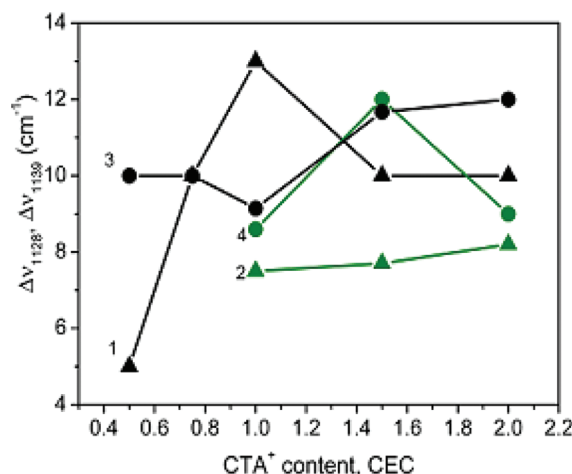


Figure 7. Band widths of the Raman bands at 1128 cm^{-1} (▲ and curves 1 and 2) and at 1139 cm^{-1} (● and curves 3 and 4) for the nonpolarized (black) and polarized (green) Raman spectra versus CTA^+ content in CTA^+-MMT .

Figure 7 shows the experimentally measured spectral widths of the Raman bands at 1128 and 1139 cm^{-1} for nonpolarized and polarized Raman spectra of CTA^+-MMT as functions of CTA^+ mass content. These widths were determined by deconvoluting the symmetric C–C stretching Raman band into the two characteristic lines at 1128 and 1139 cm^{-1} . We have observed considerable differences between the values of the 1128 cm^{-1} line width for the nonpolarized and polarized Raman spectra (compare curves 1 and 2 in Figure 7). Also, the values of the 1139 cm^{-1} line width are observed to be different for the nonpolarized and polarized Raman spectra of CTA^+-MMT at CTA^+ ion content of 2.00 CEC (see curves 3 and 4 in Figure 7). These experimental observations suggest that more than two lines could contribute to the line shape of the band mainly determined by the symmetric C–C stretching Raman mode. Therefore, we have tried to perform the deconvolution of the symmetric C–C stretching Raman band by three lines or more. However, no indication for additional lines could be found.

3.5. Further Evidence for the Doublet Assignment – Quantitative and Qualitative Analysis of the Conformational Order. As was already mentioned in the Introduction, low-intensity bands with wavenumbers at 1126 and 1142 cm^{-1} were observed previously in the Raman spectrum of CTAB micellar form.¹³ The Raman spectrum of micellar CTAB given in ref 13 contained also the high-intensity band at about 1084 cm^{-1} , which is attributed to the asymmetric stretching vibrations of C–C bonds in CH_2 -chains with numerous *gauche*-conformers.^{15,19} With this knowledge about micellar CTAB showing the prominent “numerous *gauche*-conformer” signature around 1084 cm^{-1} , we have carried out a quantitative analysis to further evidence our assignment of the Raman lines at 1128 and 1139 cm^{-1} to vibrations in *trans*-segments within CTA^+-MMT composites. For this purpose, we have evaluated, for the CTA^+-MMT hybrids, the following quantitative structural characteristics: the number $a_{\text{trans-I}}$ of *trans*-segments $-(\text{CH}_2)_k-\text{N}^+-(\text{CH}_3)_3$ with $k = 12-15$ (*trans*-segments of type I), the number $a_{\text{trans-II}}$ of *trans*-segments $-(\text{CH}_2)_k-$ with $k = 6-8$ (*trans*-segments of type II), and the total number $a_{\text{total-trans}}$ of *trans*-segments in CH_2 -chains. These structural characteristics were calculated from the nonpolarized Raman spectra using the following formulas, in

analogy to the already established formula for the quantification of *trans*-segments in our previous study on DDA⁺–MMT hybrids.⁷

$$\alpha_{\text{total-trans}} (\%) = \gamma_1 \frac{I_{1064}}{I_{1295}(\text{CH}_2)} \times 100\% \quad (5)$$

$$\alpha_{\text{trans-I}} (\%) = \gamma_2 \frac{I_{1128}}{I_{1295}(\text{CH}_2)} \times 100\% \quad (6)$$

$$\alpha_{\text{trans-II}} (\%) = \gamma_3 \frac{I_{1139}}{I_{1295}(\text{CH}_2)} \times 100\% \quad (7)$$

Here, I_{1064} , I_{1128} , I_{1139} , and I_{1295} (CH_2) are the integral intensities of the Raman bands at 1064, 1128, 1139, and about 1295 cm^{-1} , respectively. The Raman band at 1064 cm^{-1} is attributed to the asymmetric stretching vibrations of C–C bonds in *trans* CH_2 -chains.^{13,15,19} The coefficients $\gamma_1 = 1.2 \pm 0.1$ and $\gamma_2 = 1.7 \pm 0.1$ were determined from the ratios $I_{1064}/I_{1295}(\text{CH}_2)$ and $I_{1128}/I_{1295}(\text{CH}_2)$, respectively, in the nonpolarized spectrum of solid CTAB under the assumption that it consists of all *trans*-sequences.²⁶ The coefficient $\gamma_3 = 1.3$ was already reported in the work by Bramibilla et al.,¹⁹ in which the local order in liquid *n*-alkanes was studied by Raman spectroscopy.

We have found that, for the CTA⁺–MMT hybrids studied in this work, the characteristic values $\alpha_{\text{total-trans}}$, $\alpha_{\text{trans-I}}$ and $\alpha_{\text{trans-II}}$ are $86 \pm 8\%$, $36 \pm 8\%$, and $36 \pm 8\%$, respectively, at all CTA⁺ ion content. An exception is the CTA⁺–MMT hybrid with CTA⁺ content of 1.00 CEC, for which the $\alpha_{\text{trans-I}}$ and $\alpha_{\text{trans-II}}$ equal 50% and 30%, respectively. This could be due, either to a non-negligible contribution of additional modes or to a possible and more pronounced difference in the symmetry of the *trans* segment types at the modifier content of 1.00 CEC.

In addition, unlike the case of CTAB micellar form, a very low intensity is observed at wavenumbers around 1084 cm^{-1} (asymmetric stretching vibrations of C–C bonds in CH_2 -chains with numerous *gauche*-conformers) in the Raman spectra of our CTA⁺–MMT hybrids. This observation is in a good agreement with the rather predominant values for the total amount of *trans*-segments $\alpha_{\text{total-trans}}$. Thus, the correctness of the estimates for the $\alpha_{\text{total-trans}}$, $\alpha_{\text{trans-I}}$, and $\alpha_{\text{trans-II}}$ further confirms our assignment of both lines at 1128 and 1139 cm^{-1} to vibrations in *trans*-segments.

The shape of the Raman spectrum in the region 1400 – 1500 cm^{-1} is sensitive to the state of packing and *trans/gauche* conformational order of CH_2 -chains.^{15,31,32} We have found that, in the region 1400 – 1500 cm^{-1} , the Raman spectra of CTA⁺–MMT hybrids and the Raman spectrum of solid CTAB differ dramatically. The broad nonresolved band with its maximum at about 1446 cm^{-1} is observed in our Raman spectra of CTA⁺–MMT hybrids instead of four narrow lines at 1398 , 1416 , 1442 , and 1467 cm^{-1} , which are observed in the spectrum of solid CTAB (Figure 3). Taking into account the high fraction of *trans*-segments in CTA⁺ ions of our modified clays as evidenced above, we consider that the appearance of the broad band at about 1446 cm^{-1} indicates a change in the packing state of CTA⁺ ion. As demonstrated in section 2.2, our DSC studies reveal that the state of CTA⁺ ions in the CTA⁺–MMT hybrids is liquid-like (no sign of CTA⁺ melting in the thermograms of CTA⁺–MMT hybrids was present at any CTA⁺ content). This confirms our conclusion about a different packing state of the CTA⁺ ions embedded in the clay interlayer space in comparison with the packing of their chains in solid CTAB.

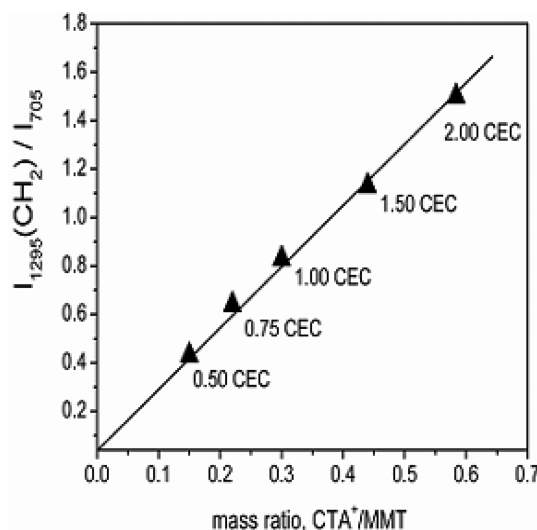


Figure 8. Integral intensity ratio $I_{1295}(\text{CH}_2)/I_{705}$ (clay) versus the mass ratio of CTA⁺ ions and clay (MMT).

3.6. Raman Estimation of the CTA⁺ Ion Content in CTA⁺–MMT Hybrids. Similar to our previous study⁷ of MMT modified by DDAB, also in our present investigation we have found that the integral intensity ratio I_{1295}/I_{705} is proportional to the mass ratio of CTA⁺ ions to MMT. In fact, the line at 705 cm^{-1} is observed only in the Raman spectra of the modified clay samples (Figure 3) and in the spectrum of neat clay (spectrum not shown), while the spectrum of solid CTAB shows no Raman line at this position. This band is attributed to the vibrational mode of the clay structural units formed by SiO₄-tetrahedrons.²⁷ Consequently, because the 1295 cm^{-1} band intensity is proportional to the total amount of CH₂ groups (both *trans* and *gauche*), the ratio $I_{1295}(\text{CH}_2)/I_{705}(\text{clay})$ in the Raman spectra of CTA⁺–MMT provides a reasonable and very reliable way to directly determine the mass content of CTA⁺ ions with respect to that of MMT.

Figure 8 shows the calibration curve comparing the values of the CTA⁺/MMT mass ratio, predicted from Raman data using the ratio $I_{1295}(\text{CH}_2)/I_{705}(\text{clay})$, and the reference values predetermined by the sample preparation (i.e., the CEC values obtained through the cation exchange chemical reaction during clay modification). These reference values were measured by an original method described in detail in an earlier work.⁴ The perfect linear fit agreement for this calibration reflects the good precision of the predetermined reference values of the CTA⁺ ion contents and also validates the reliability of the present Raman measurements.

4. CONCLUSIONS

Sodium montmorillonite clay modified with variable mass contents of cetyltrimethylammonium bromide (CTAB) has been studied using theoretical simulations and by Raman spectroscopy in the spectral region 600 – 1600 cm^{-1} . Our earlier findings from the investigations of clay modified by other alkylammonium salts and computer-simulation modeling have helped to refine the interpretation of the present results and to reach interesting and consistent conclusions.

As we have reported in our previous Raman studies on sodium montmorillonite modified by other alkylammonium salts, we have found a very interesting behavior associated with the band

splitting of the symmetric C–C stretching mode of *trans*-segments. This band, observed at 1128 cm^{−1} in the Raman spectrum of solid CTAB, splits into two sub-bands, forming a characteristic doublet with wavenumbers at 1128 and 1139 cm^{−1} in the spectra of clays modified by CTAB. We have shown that this splitting appears when two types of *trans*-segments in CH₂ chains coexist. These two types of *trans*-segments differ in their chemical composition and length. A *trans* segment of the first type is a sequence of $-(\text{CH}_2)_k-$ with $k = 12–15$, ending with the terminal (CH₃)₃–N– unit. The *trans*-segment of the second type contains 6–8 CH₂-groups without the terminal (CH₃)₃–N– unit and has been demonstrated to appear as a result of the bending of the CH₂ chains in the alkylammonium ions embedded within the clay interlayer space. The characteristic Raman doublet bands at wavenumbers 1128 and 1139 cm^{−1} have been attributed to vibrations of the first and second *trans*-segment types, respectively. By monitoring the integral intensity ratios $I_{1128}/I_{1295}(\text{CH}_2)$ and $I_{1139}/I_{1295}(\text{CH}_2)$, we have quantified the contents of these two types of *trans*-segments. We have found that, within CTA⁺–MMT hybrids, the first and second types of *trans*-segments coexist at any modifier content from 0.50 to 2.00 CEC in approximately equal proportions.

In addition, by monitoring the integral intensity ratio $I_{1064}/I_{1295}(\text{CH}_2)$ and the spectral features in the region 1400–1500 cm^{−1}, we have shown that the total content of *trans*-segments in the clay modified by CTAB is high enough, $\sim 86 \pm 8\%$, at any modifier content. However, the packing of the modifier ions embedded within the clay interlayer space differs considerably from their packing in the monocrystal of CTAB. This has been fully supported by the Raman spectroscopy-based evidence of the existence of the symmetric C–C stretching doublet associated with CH₂-chain length and chemical dissimilarities within CTA⁺–MMT hybrids, as a result of CH₂-chain bending. Therefore, the conformation related information present in our Raman spectra has helped to judge available computer-simulated models and to select realistic models, which, for example, best describe the packing state of the CTA⁺ within CTA⁺–MMT hybrids.

Furthermore, we have shown that the integral intensity ratio $I_{1295}(\text{CH}_2)/I_{705}(\text{clay})$ in the Raman spectra of clay modified by CTAB can be used for the quantitative prediction of the relative mass content of modifier molecules (alkylammonium ions CTA⁺) embedded in the clay interlayer space. The predicted CTA⁺/MMT mass ratios are in a perfect and linear calibration agreement with the corresponding reference values measured by an original method during sample preparation. Moreover, we have further explained the phenomenon associated with the splitting of the symmetric C–C stretching Raman-active mode by additionally analyzing the behavior of this mode in the Raman spectra of *n*-alkanes and different alkylammonium substances (primary *n*-alkylamines, CTAB, DODAB, DDAB). We have demonstrated that the wavenumber of the symmetric C–C stretching Raman-active mode in *trans*-segments of CH₂-chain depends on both the mass of the terminal group and the length of the CH₂-chain. In particular, because of the presence of a heavy terminal group $-\text{N}^+\text{H}_3$ in primary *n*-alkylamines, the dispersion wavenumber law for the symmetric C–C stretching mode as a function of the length of CH₂-chain differs from the law suggested by Gorelik and coworkers^{22,28} for *n*-alkanes.

Our results yield new insights into unique conformational reorganization associated with the behavior of the symmetric C–C stretching mode in the Raman spectra of clay-based alkylammonium systems, suggesting a generalized formalism based

on chain bending resulting in specific conformational states of embedded organic molecules within confined nanosized galleries of clay. These results also demonstrate the capability of Raman spectroscopy for a straightforward rapid and nondestructive quantification of the specific modifier-dependent interlayer conformational states, making this technique an important tool for a tunable fabrication of modified clay-based nanocomposites with desired properties.

■ AUTHOR INFORMATION

Corresponding Author

*Tel.: 0074995038768. Fax: 0074991352055. E-mail: sagitova@kapella.gpi.ru.

■ ACKNOWLEDGMENT

This work is supported by the Russian Foundation for Basic Research (09-02-00587-a), the Grant of the President of the Russian Federation for Leading Scientific Schools (3675.2010.2). E.A.S. acknowledges support by INTAS (Project No. 06-1000014-6055), by the German Academic Exchange Service (DAAD, Project No.A/10/01059), and by the International Center for Transdisciplinary Science at Jacobs University Bremen. P.D. acknowledges a Ph.D. grant (04/2006-09/2009) by DAAD.

■ REFERENCES

- (1) Chen, X.; Hu, N.; Zeng, Y.; Rusling, J. F.; Yang, J. *J. Langmuir* **1999**, 15, 7022–7030.
- (2) Alexandre, M.; Dubois, P. *Mater. Sci. Eng.* **2000**, 28, 1–63.
- (3) Antipov, E. M.; Guseva, M. A.; Gerasin, V. A.; Korolev, Y. M.; Rebrov, A. V.; Fischer, H. R.; Razumovskaya, I. V. *Polym. Sci., Ser. A* **2003**, 45, 1130–1139.
- (4) Gerasin, V. A.; Bakhov, F. N.; Merekalova, N. D.; Korolev, Y. M.; Fischer, H. R.; Antipov, E. M. *Polym. Sci., Ser. A* **2005**, 47, 954–967.
- (5) Schleidt, S.; Spiess, H. W.; Jeschke, G. *Colloid Polym. Sci.* **2006**, 284, 1211–1219.
- (6) Boutafat, M.; Ait-Amar, H.; McWhinnie, W. R. *Desalination* **2007**, 206, 394–406.
- (7) Sagitova, E. A.; Donfack, P.; Prokhorov, K. A.; Nikolaeva, G. Yu.; Gerasin, V. A.; Merekalova, N. D.; Materny, A.; Antipov, E. M.; Pashinin, P. P. *J. Phys. Chem. B* **2009**, 113, 7482–7490.
- (8) Vaia, R. A.; Teukolsky, R. K.; Giannelis, E. *Chem. Mater.* **1994**, 6, 1017–1022.
- (9) Prokhorov, K. A.; Sagitova, E. A.; Nikolaeva, G. Y.; Kozlov, D. N.; Pashinin, P. P.; Antipov, E. M.; Gerasin, V. A.; Bakhov, F. N.; Guseva, M. A. *Laser Phys. Lett.* **2005**, 2, 285–291.
- (10) He, H.; Frost, R. L.; Xi, Y.; Zhu, J. *J. Raman Spectrosc.* **2004**, 35, 316–323.
- (11) Osman, M. A.; Seyfang, G.; Suter, U. W. *J. Phys. Chem. B* **2000**, 104, 4433–4439.
- (12) Okuayma, K.; Iijima, N.; Hirabayashi, K.; Kunitake, T.; Kusunoki, M. *Bull. Chem. Soc. Jpn.* **1988**, 61, 2337–2341.
- (13) Kalyanasundaram, K.; Thomas, J. K. *J. Phys. Chem.* **1976**, 80, 1462–1473.
- (14) Okuayma, K.; Soboi, Y.; Iijima, N.; Hirabayashi, K.; Kunitake, T.; Kajiyama, T. *Bull. Chem. Soc. Jpn.* **1988**, 61, 1485–1490.
- (15) Strobl, G. R.; Hagedorn, W. *J. Polym. Sci., Polym. Phys. Ed.* **1978**, 16, 1181–1193.
- (16) Snyder, R. G.; Cameron, D. G.; Casal, H. L.; Compton, D. A.C.; Mansch, H. H. *Biochim. Biophys. Acta* **1982**, 684, 111–116.
- (17) Amorim da Costa, A. M.; Geraldes, C. F. G. C.; Teixeira-Dias, J. J. C. *J. Raman Spectrosc.* **1982**, 13, 56–62.

- (18) Amorin da Costa, A. M.; Batista de Carvalho, L.A. E.; Barbosa, E. F. G.; Teixeira-Dias, J. J. C.; Lampreia, I. M. S. *Can. J. Chem.* **1987**, 65, 384–390.
- (19) Brambilla, L.; Zerbi, G. *Macromolecules* **2005**, 38, 3327–3333.
- (20) Schachtschneider, J. H.; Snyder, R. G. *Spectrochim. Acta* **1963**, 19, 117–168.
- (21) Koboyashi, M.; Koizumi, H.; Cho, Y. *J. Chem. Phys.* **1990**, 93, 4659–4672.
- (22) Gorelik, V. S.; Zlobina, L. I.; Sharts, O. N. *Proc. SPIE* **2000**, 4203, 66–77.
- (23) Gall, M. J.; Hendra, P. J.; Peacock, C. J.; Cudby, M. E. A.; Wills, H. A. *Spectrochim. Acta, Ser. A* **1972**, 28, 1485–1496.
- (24) Kint, S.; Scherer, J. R.; Snyder, R. G. *J. Chem. Phys.* **1980**, 73, 2059–2062.
- (25) Snyder, R. G. *J. Chem. Phys.* **1967**, 47, 1316–1360.
- (26) He, H.; Frost, R. L.; Bostrom, Th.; Yang, P.; Duong, L.; Xi, Y.; Klopogge, J. T. *Appl. Clay Sci.* **2006**, 31, 262–271.
- (27) Frost, R. L.; Rintoul, L. *Appl. Clay Sci.* **1996**, 11, 171–183.
- (28) Gorelik, V. S. Idealized models of crystalline chains. In *Inelastic Light Scattering in Crystals*; Sushchinsky, M. M., Ed.; Nova Science Publishers: New York, 1989; Vol.180, pp 100–135.
- (29) Kohlrausch, K. W. F. *The Raman Spectra*; The Foreign Literature Press (Russ. Transl.): Moscow, USSR, 1952. Kohlrausch, K. W. F. *Ramanspektren*; Akademische Verlagsgesellschaft; Leipzig, 1943.
- (30) Venkataraman, N. V.; Vasudevan, S. *J. Phys. Chem. B* **2001**, 105, 1805–1812.
- (31) Wang, W.; Gu, B.; Liang, L.; Hamilton, W. *J. Phys. Chem. B* **2004**, 108, 17477–17483.
- (32) Abbate, S.; Zerbi, G.; Wunder, S. L. *J. Phys. Chem.* **1982**, 86, 3140–3149.